Steel and Composite Structures, *Vol. 27, No. 4 (2018) 495-508*
DOI: https://doi.org/10.12989/scs.2018.27.4.495

Shear behavior of composite frame inner joints of SRRC column-steel beam subjected to cyclic loading

Hui Ma [*1,2], Sanzhi Li [1], Zhe Li [1], Yunhe Liu [1,2], Jing Dong [1] and Peng Zhang [1]

[1] *School of Civil Engineering and Architecture, Xi'an University of Technology, Xi'an, China*
[2] *State Key Laboratory Base of Eco-hydraulic Engineering in Arid Area, Xi'an University of Technology, Xi'an, China*

(*Received August 30, 2017, Revised January 15, 2018, Accepted March 24, 2018*)

Abstract. In this paper, cyclic loading tests on composite frame inner joints of steel-reinforced recycled concrete (SRRC) column–steel beam were conducted. The main objective of the test was to obtain the shear behavior and analyze the shear strength of the joints. The main design parameters in the test were recycled coarse aggregate (RCA) replacement percentage and axial compression ratio. The failure process, failure modes, hysteresis curves and strain characteristics of the joints were obtained, and the influences of design parameters on the shear strength of the joints have been also analysed in detail. Results show that the failure modes of the joints area are typical shear failure. The shear bearing capacity of the joints maximally decreased by 10.07% with the increase in the RCA replacement percentage, whereas the shear bearing capacity of the joints maximally increased by 16.6% with the increase in the axial compression ratio. A specific strain analysis suggests that the shear bearing capacity of the joints was mainly provided by the three shear elements of the recycled aggregate concrete (RAC) diagonal compression strut, steel webs and stirrups of the joint area. According to the shear mechanism and test results, the calculation formulas of the shear bearing capacity of the three main shear elements were deduced separately. Thus, the calculation model of the shear bearing capacity of the composite joints considering the adverse effects of the RCA replacement percentage was established through a superposition method. The calculated values of shear strength based on the calculation model were in good agreement with the test values. It indicates that the calculation method in this study can reasonably predict the shear bearing capacity of the composite frame inner joints of SRRC column–steel beam.

Keywords: SRRC columns; steel beams; composite frame; inner joints; shear bearing capacity; cyclic loading

1. Introduction

The rapid development of the construction industry had caused numerous negative influences on the ecological environment. On the one hand, the concrete construction of massive new buildings required the consumption of large quantities of natural coarse aggregate (NCA), thereby directly leading to an excessive exploitation of the NCA. On the other hand, many old buildings were demolished, thus producing large amounts of construction wastes that not only occupied a considerable land but also polluted the environment. Therefore, using recycled aggregate concrete (RAC) as a new type of product material was proposed to reduce the negative influences and the amount of NCA used in concrete construction (Xu *et al*. 2017, Xiao 2008, Poon *et al*. 2002, Chen *et al*. 2003, Huda and Alam 2014). RAC is a type of green concrete that was made from the waste concrete of old buildings which were composed partly or completely of recycled coarse aggregates (RCA) instead of NCA and has a broad development and application prospect. It positively contributes to the sustainable development of the concrete industry and has been recognized as an effective method for solving environmental problems.

In recent years, the RAC has captured the interest of many scholars and has been widely investigated around the world. Most studies showed that the mechanical properties of RAC, such as strength, deformation, elastic modulus and durability, are different from those of ordinary concrete (Xiao 2008, Huda and Alam 2014, Šeps *et al*. 2016, Silva *et al*. 2016, Thomas *et al*. 2013). In addition, several studies on the RAC structural members have also been conducted (Ignjatović *et al*. 2017, Chen *et al*. 2017, Ma *et al*. 2013, 2015, Wu *et al*. 2013, Xue *et al*. 2014, Bao 2014, Marthong *et al*.2017, Gonzalez and Moriconi 2014). Major findings show that the final failure modes of RAC members are similar to that of ordinary concrete members, but the bearing capacity and ductility of the RAC structures decrease gradually with the increase of RCA replacement percentage. However, the RAC material that was designed based on a reasonable mixture ratio can be applied to the structural members or structures (Rosado *et al*. 2017, Senaratne *et al*. 2017, Xue *et al*. 2010, Breccolotti and Materazzi 2010, Yoda and Shintani 2014).

The composite structures of steel and concrete can effectively reflect the advantages of the mechanical properties of the two materials. Several researchers have successively studied the mechanical properties of the composite members of steel and RAC considering this advantage (Ma *et aal*. 2013, 2015, Wu *et al*.2013, Xue *et al*.

∗Corresponding author, Ph.D., Associate Professor,
E-mail: mahuiwell@163.com

http://www.techno-press.org/?journal=scs&subpage=6
ISSN: 1229-9367 (Print), 1598-6233 (Online)

2014). The authors have systematically studied the seismic performance of steel-reinforced recycled concrete (SRRC) columns in detail (Ma *et al*. 2013, 2015, 2016). The results show that the SRRC columns have a higher bearing capacity and better seismic performance than the reinforced recycled concrete columns. Based on this result, using an SRRC column–steel beam composite frame combined with the characteristics of a steel beam, that is, favourable mechanical performance, light quality and simple construction, is proposed in this paper. The new composite frame possesses the characteristics not only of SRRC column and steel beam, but also of the RAC that has energy-saving and environmental protection properties. It is a kind of green structure and has a broad development and application prospect. In addition, the joints are the key parts of the frame structure. The joint in the frame structure will be influenced by the combined force of pressure, shear force and bending moment when external loads act on the frame structure. The force mechanism of the joint is complicated. Therefore, the joints must be considered seriously in designing the composite frame. Currently, several studies on the reinforced recycled concrete joints (Marthong *et al*. 2017, Gonzalez and Moriconi 2014), recycled concrete-filled steel tube frame joints (Wu *et al*. 2013, Yang 2015) and SRRC frame joints (Xue *et al*. 2014, Bao 2014) have been conducted and showed positive and encouraging results on the RAC material. However, few studies have been conducted on the shear behavior and calculation method of shear strength of the composite frame joints of SRRC column–steel beam.

Therefore, the seismic performance and shear behavior of the five composite frame inner joints of SRRC column – steel beam were investigated under cyclic loading test. The influence rules of the RCA replacement percentage and axial compression ratio on the shear behavior of the joints were analysed and summarized in detail. The calculation model and method of the shear bearing capacity of the joints were established and verified based on the test and analysis results. The conclusions can provide a reference for applying this type of frame joints.

2. Experimental procedures

2.1 Materials and mixture proportions

Five specimens of the frame joints were designed and fabricated in the test. Profile steel of Q235 was adopted and HRB335 ribbed rebars with diameters of 8 and 14 mm were adopted for transverse stirrups and longitudinal rebars, respectively. Table 1 lists the mechanical properties of the profile steel and the rebars that were adopted in the test. In addition, ordinary Portland cement (C) with the compressive strength grade of 42.5 MPa was used in the investigation. The NCA was composed of artificially crushed natural aggregate with a favourable gradation. The RCA was obtained by crushing waste concrete blocks from demolished old buildings. The grain sizes, gradation and physical properties of the RCA can satisfy the requirements of Chinese code GB/T25177-2010, that is, RCA for concrete. The 28-day cubes compressive strength of the RAC that was prepared in the test was approximately 40 MPa. Moreover, ordinary river sand was used as fine aggregate. The preparation process of the RAC requires mixing this material with a certain amount of fly ash and water-reducing agent to improve the workability of this material. The mix ratio and basic mechanical properties of the RAC material are illustrated in Table 2.

Table 1 Mechanical properties of the profile steel and the rebars in the joints

Steel products		Yield strength f_y /MPa	Ultimate strength f_u /MPa	Elastic modulus E_s /MPa	Yield strain $\mu\varepsilon$
Steel in column	Flange	329.8	465.8	2.02×10^5	1632
	Web	391.5	503	1.99×10^5	1967
Steel beam	Flange	268.3	443.6	1.93×10^5	1390
	Web	329.8	465.8	2.02×10^5	1632
Longitudinal rebars	⌀14	446.3	523.8	2.15×10^5	2075
Stirrups	⌀8	418.9	491.6	2.12×10^5	1976

Table 2 Mix proportions and mechanical properties of the RAC material

RAC strength grade	r (%)	Unit weight (kg/m^3)						f_{rcu} (MPa)	f_{rc} /(MPa)	f_t (MPa)	E_{rc} (MPa)
		W/C	W	C	S	NCA	RCA				
C40	0	0.43	195	464	585	1187	0	45.98	34.94	2.89	2.533×10^4
C40	50	0.43	195	464	585	593.5	593.5	44.46	33.79	2.83	2.508×10^4
C40	100	0.43	195	464	585	0	1187	40.65	30.89	2.67	2.440×10^4

*Note: f_{rcu} -Compressive strength of cubes; f_{rc} -Axial compressive strength of prismatic cylinder;
f_t -Tensile strength; E_{rc} -elastic modulus

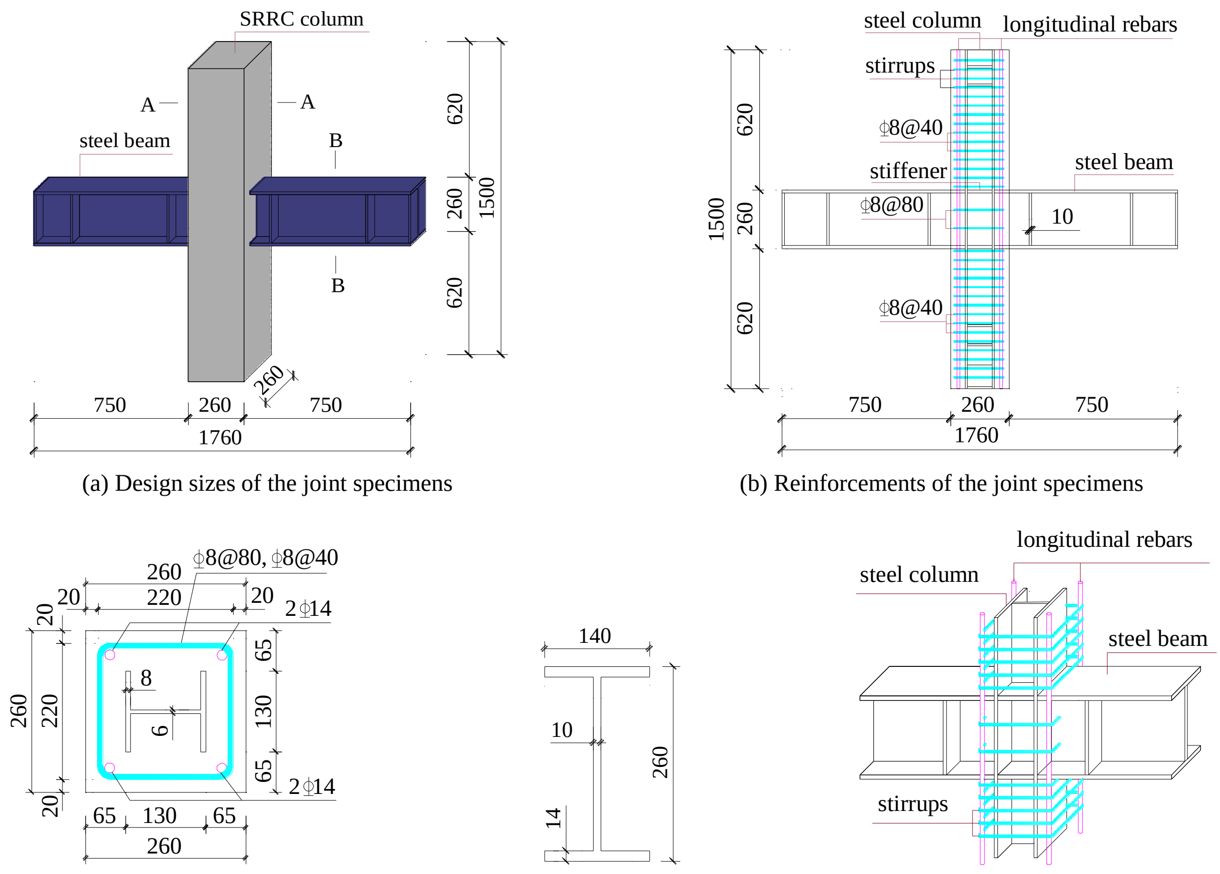

(a) Design sizes of the joint specimens

(b) Reinforcements of the joint specimens

(c) Cross section of A-A

(d) Cross section of B-B

(e) Reinforcements of joints

Fig.1 The design sizes and reinforcements of joints

Table 3 Design parameters of the joint specimens

Specimen number	RAC strength grade	Axial compression ratio n	RCA replacement percentage r/%	Profile steel ratio/%	Stirrup ratio /%	Joint forms
CFJ1	C40	0.36	0	4.8	1.26	Inner joint
CFJ2	C40	0.36	50	4.8	1.26	Inner joint
CFJ3	C40	0.36	100	4.8	1.26	Inner joint
CFJ4	C40	0.18	100	4.8	1.26	Inner joint
CFJ5	C40	0.54	100	4.8	1.26	Inner joint

*Note: CFJ- Composite frame joint

2.2 Design and fabrication of specimens

In the joint specimens, the cross-section size for the SRRC columns was 260 mm × 260 mm and the height was 1500 mm. The SRRC column was equipped with solid webs I-steel and four longitudinal rebars and reinforced transversely with multiple stirrups. Two stirrups were arranged in the joint area (80 mm spacing), whereas the stirrups positioned on the remaining part of the column were encrypted (40 mm spacing). The design sizes and reinforcements of specimens are depicted in Fig. 1. The steel beams were welded on both sides of the steel flanges of the profile steel in the SRRC columns with a length of 750 mm on each side. The two design parameters, namely, axial compression ratio and RCA replacement percentage, were considered, and their values are presented in Table 3. The RCA replacement percentage (i.e., 0%, 50%, and 100%) is the ratio of the RCA mass to the mass of all the coarse aggregates. The axial compression ratio n of the joints can be calculated using $n = N/(f_{rc}A_c + f_yA_s)$. In addition, the volume stirrup ratio and profile steel ratio of all the specimens were about 1.26% and 4.8%, respectively.

2.3 Measuring points arrangement

In the test, nine displacement meters were used in each specimen to measure the displacement of the corresponding parts. DM-1–DM-5 displacement meters were installed along the centerline of the loading cross section of the specimens to monitor the in-plane lateral displacement in

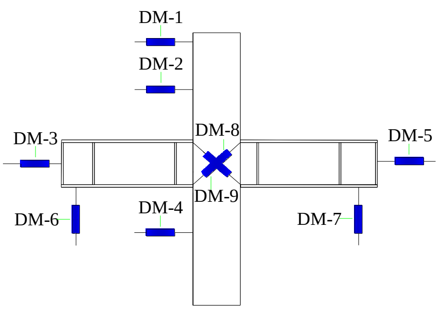

(a) Arrangement of displacement meters

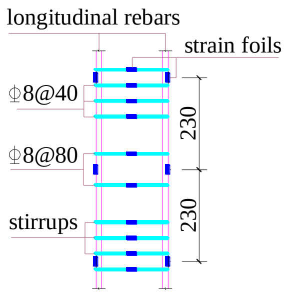

(b) Arrangement of strain foils on the rebars

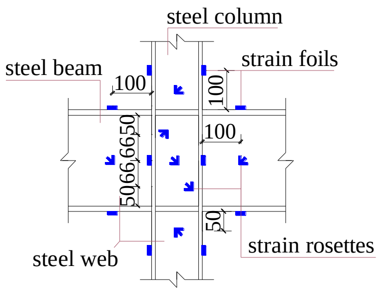

(c) Arrangement of strain foils on the steel webs

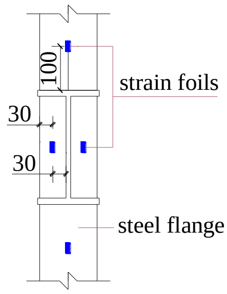

(d) Arrangement of strain foils on the steel flanges

Fig. 2 Arrangement of displacement meters and strain foils in the joints

various parts of the joints. DM-6–DM-7 displacement meters were placed at the bottom of steel beam ends along the centerline of the cross section to measure the in-plane vertical displacement of steel beams. The shear deformation of the joints was measured using two cross-displacement meters (DM-8–DM-9) which were located in the joint area. The arrangement of the displacement meters is shown in Fig. 2(a). In addition, the strain foils and rosettes were also positioned on the steel webs, steel flanges, stirrups and longitudinal rebars in the joint areas to measure their strain. The arrangements of the strain foils or strain rosettes on the rebars, steel webs and steel flanges are exhibited in Figs. 2(b)-(d).

2.4 Test devices and loading program

The cyclic loading tests were performed using the MTS electro-hydraulic servo test machine in the Laboratory of Structural Engineering at the Xi'an University of Technology in China. The test simulates shear behavior of the composite frame inner joints of SRRC column–steel beam subjected to horizontal earthquakes. Fig. 3 illustrates the test setup of the cyclic loading tests in this paper. The axial compression load during the test was first applied to the top of SRRC column to a predetermined value in accordance with the axial compression ratio and then was stabilized. The lateral cyclic loads were applied to the loading point of the specimens by using the MTS test machine. The ground beams of the test setup were secured to the ground grooves using eight anchor bolts to prevent the ground beams from sliding under the cyclic loads. The force diagram of the joints is depicted in Fig. 4. The Code for Seismic Test Method of Buildings in China states that the loading program of the cyclic loading test involved in two main load steps, namely, a load-controlled step and a displacement-controlled step, as demonstrated in Fig. 5. The specimens of the joint were subjected to the load-controlled loading program before yielding. After the specimens

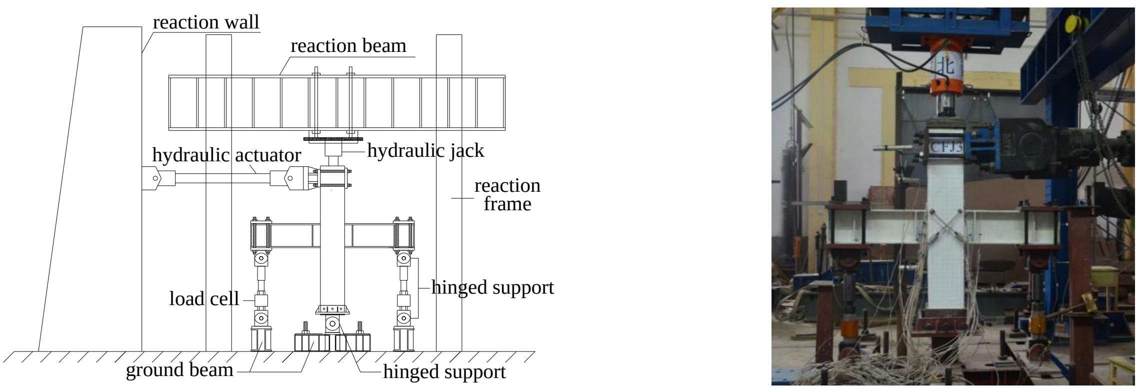

Fig. 3 Test setup of the composite joints under cyclic loading

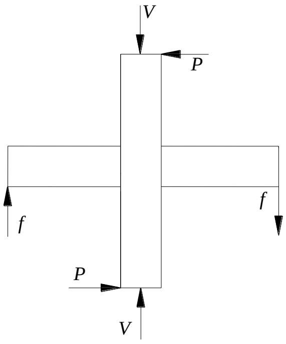

Fig. 4 Force diagram of the joints

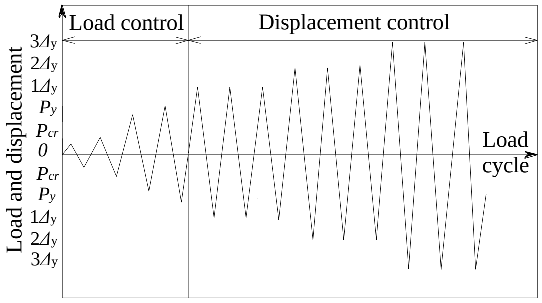

Fig. 5 Loading program of test

yielding, the displacement-controlled method was performed by the multiple of yield displacement. In addition, each displacement-controlled step was repeated thrice until the lateral loads dropped below the 85% peak value or when the specimens can no longer bear the load. The rate of loading and unloading was similar during the cyclic loading test. The whole loading and data collection process was controlled by a computer.

3. Results and analysis

3.1 Failure process and modes

Based on the failure characteristics of the five joint specimens subjected to cyclic loading, the failure modes of the joints were mainly typical shear failure in the joint area. The failure process of the joints was divided into three main stages, namely, elastic stage, working with crack stage and failure stage. The two design parameters of the axial compression ratio and RCA replacement percentage had a slight effect on the failure modes. In this study, CFJ5 specimen was used to describe the failure process and characteristic of the joints, as exhibited in Fig. 6.

(1) Elastic stage: in the early stage of loading, no obvious crack was observed in the joint area. A few small horizontal cracks appeared in the lower part of the joints area when the lateral load increased to approximately 50 kN. Many other cracks continued to appear on both sides of the joint area as the lateral load continued to increase, and the original cracks gradually extended but with a short width. The strains of the joint components and steel beam ends on both sides of the joint areas were very small and varied linearly as load increased, thereby showing that the composite joints were basically in the elastic stage.

(2) Working with crack stage: the diagonal cracks were found in the middle part of the joint area

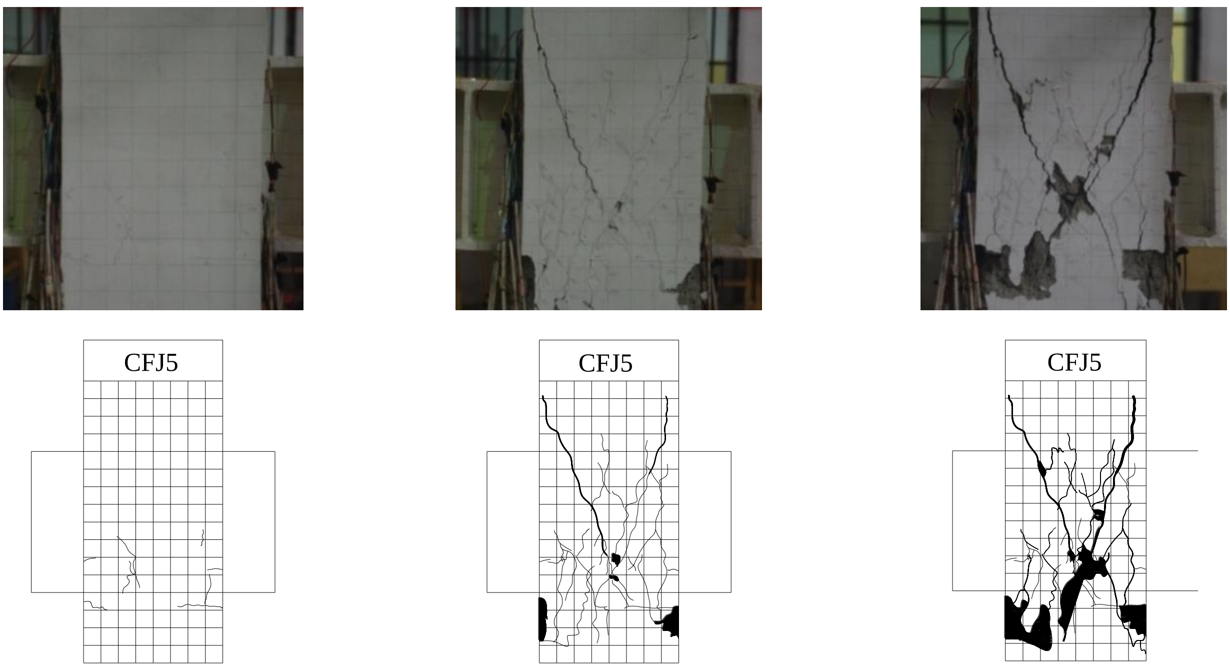

(a) Elastic stage (b) Working with crack stage (d) Failure stage

Fig. 6 Failure process of the CFJ5

when the lateral load was loaded to approximately 80 kN. The diagonal cracks were constantly generated and extended in the joint area as the load increased, whereas the horizontal cracks extended slowly. The diagonal cracks spread into X-shaped cross cracks in the middle part of the joint area when the horizontal loads reached 100 kN, and the width of the cross cracks increases gradually. Meanwhile, the RAC in the specimen of the joint area was separated into numerous diamond-shaped blocks.

(3) Failure stage: The steel webs in the core area of the joint began to yield when the lateral load reached 110 kN, and the strain of the stirrups gradually increased. At this point, the specimen reached the yield and then loading with the displacement-controlled step. The original diagonal cracks in the joint area continuously extended when the controlled displacement was increased to 24 mm. The tearing sound of the RAC originated from the joint area, and the RAC cover of the rebars began to collapse. Several small pieces of RAC in the middle part of joint area collapsed when the cyclic displacement was controlled to 32 mm. The steel webs yielded completely, and several stirrups began to yield. After that, the horizontal bearing capacity of the joints began to decline. The RAC diamond-shaped blocks in the core of the joint area collapsed when the horizontal loads dropped to 85% of the peak loads, and the steel webs entered the strengthening stage, and certain stirrups yielded. At this point, the strain of the steel beam ends remained relatively small and did not reach the yield. Finally, the specimens were damaged because of the significant decrease in the bearing capacity.

3.2 Hysteresis curves

Fig. 7 displays the hysteresis curves of the joints which trace the relationship of lateral loads and displacements of the top of the SRRC columns in the joints. In Fig. 7, the hysteresis curves of all the joints were spindle-shaped and plump, thus suggesting that the joints demonstrate a favourable energy dissipation capacity. The hysteresis curves of the joints at the early stage of loading were close to a linear relationship, and the area surrounded by the hysteresis curves was narrow, thereby indicating that the energy dissipation capacity of the joints at this stage was very small. In addition, no residual deformation was observed and the stiffness was basically not degraded after unloading, thereby showing that the joints were nearly in

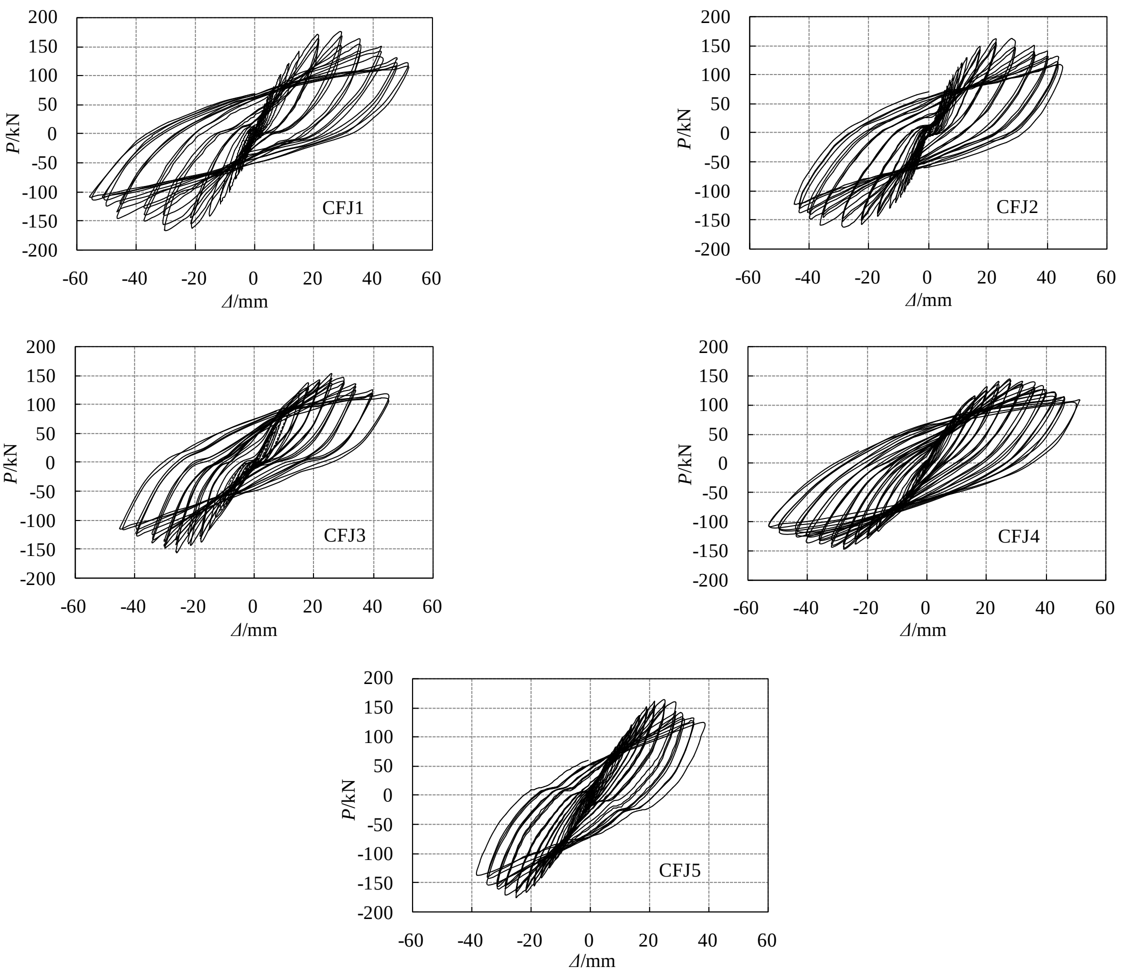

Fig. 7 Load-displacement of hysteresis curves for the joints

the elastic stage. The cracks gradually emerged in the joint area whilst the lateral cyclic loads increased, the hysteresis curves were no longer in a linear relationship, and the slopes of these curves gradually decreased. By contrast, the area surrounded by the hysteresis curves gradually increased, thus denoting that the energy dissipation capacity of the joints began to increase. At this point, the joints were in an elastic-plastic state. The displacement-controlled step was adopted after the joints yielded, and each displacement-controlled step was repeated thrice. The strength of the joints under the same displacement level was lower in the latter two cycles than in the first cycle, and the area surrounded by each cycle was gradually reduced, thereby indicating that the joints occurred stiffness degradation and the energy dissipation capacity of joints was reduced. It is mainly due to the influence of the damage accumulation in the joints under cyclic loading. The RAC in the joint area collapsed after the joints entered the failure stage. At this point, the shear bearing capacity of the joints was mainly provided by steel webs and stirrups in the joint area.

In addition, the horizontal peak loads of the joints gradually decreased with the increase in the RCA replacement percentage. The maximum decreasing amplitude of the peak loads was 10.07%, thereby indicating that the RCA replacement percentage is unfavourable to the shear bearing capacity of the joints. This phenomenon might be that the result of the internal damages of the RCA in the RAC material whilst in the process of preparation, or an old mortar might be attached to the surface of the RCA, thus leading to insufficient adhesion between the old and new mortars. Moreover, the increase in the axial compression ratio increased the bearing capacity of the joints with a maximum increment of 16.61%. Therefore, increasing properly the axial compression ratio to the shear strength of the joints is slightly advantageous.

3.3 Strain analysis and shear strength proportion in joints

The strain of the profile steel and rebars are depicted in Figs. 8-11. The strain law and shear characteristics of the joint area were studied by analyzing the strains of steel webs, steel flanges, longitudinal rebars and stirrups in this area, and the shear force contribution of the main shear elements in the joint area was also obtained.

Figs. 8-11 demonstrate that the strain of the profile steel and rebars was very small before reaching the crack load, thereby indicating that the profile steel and rebars at this point only contributed to a small portion of the shear force, whereas the RAC mainly contributed to the majority of shear force in the joint area. The strain of the profile steel and rebars of the joint area gradually increased when the joints reached the yield state, and the steel webs began to yield, the average strain of the steel webs was about 1919$\mu\varepsilon$, thereby suggesting that the shear force proportion of the profile steel and rebars gradually increased. The steel webs of joint area completely yielded when the joints reached the peak load, and the strain of the stirrups rapidly grew but did not completely yield, its average strain was about 1426$\mu\varepsilon$. At this point, the strain of the steel flanges and longitudinal rebars increased slowly, thus indicating that the shear force proportion of the steel webs and stirrups was further increased. The shear failure occurred in joints when the ultimate load was reached, and the steel webs entered the strengthening stage, the average strain of the steel webs was about 7641$\mu\varepsilon$. At this point, several stirrups of the joint area reached the yield state, and the steel flanges and longitudinal rebars in the joint area also locally yielded. Subsequently, the frame joints gradually lost their bearing capacity given the drop of the RAC in the joint area. However, the decrease rate of the bearing capacity of the joint was relatively gradual, thereby denoting that the joints maintained a high bearing capacity and favourable deformation capacity at the later stage of loading.

Clearly, steel webs and several stirrups in the joint area completely yielded when the lateral loads reached the peak load, whereas the strain of the longitudinal rebars and steel flanges were relatively small. At this point, the RAC in the joint area was crushed and gradually dropped. This observation shows that the steel webs, stirrups and RAC in the joint area play a major role in resisting the shear force, that is, these components were the main shear elements of the joints. Based on this analysis, the test values of the shear force of the joints and the main shear elements can be obtained. Under the constant axis stress and lateral loads together action on the joints, the test value V_j^t of the horizontal shear force in the joint area was calculated by the Eq. (1). The shear force V_w^t of the steel webs in core area of the joint and the shear force V_{sv}^t of the stirrups were calculated by the Eqs. (2) and (3), respectively. The shear force V_{rc}^t of RAC in the joint area was calculated by the Eq. (4). Table 4 lists the test values of the shear force of the joint at characteristic loads and the shear force proportion of the main shear elements in the joint. The characteristic loads in Table 4 include crack load P_{cr}, yield load P_y and peak load P_m, of which P_y can be obtained by the general yield bending moment method, whilst P_{cr} and P_m were determined by the test data.

$$V_j^t = \frac{M_{bl} + M_{br}}{h_b - h_f} - V \tag{1}$$

$$V_w^t = \frac{I_w t_w}{S_w} \tau_w \tag{2}$$

where $\tau_w = G_W \gamma_W$; ; $G_w = \dfrac{E}{2(1+\mu)}$

$$V_{sv}^t = aE_{sv}\bar{\varepsilon}_{sv}A_{sv1} \tag{3}$$

$$V_{rc}^t = V_j^t - V_w^t - V_{sv}^t \tag{4}$$

In Eqs. (1)-(4), M_{bl} and M_{br} are the bending moment of the beam end on the left and right sides of the joint, respectively; h_b and h_f are the height of the steel beam and the thickness of the flanges of steel beam, respectively; V_c is the horizontal force of each stage; t_w and I_w are the thickness and the section moment of inertia of the steel webs in the joint column, respectively; S_w is the area

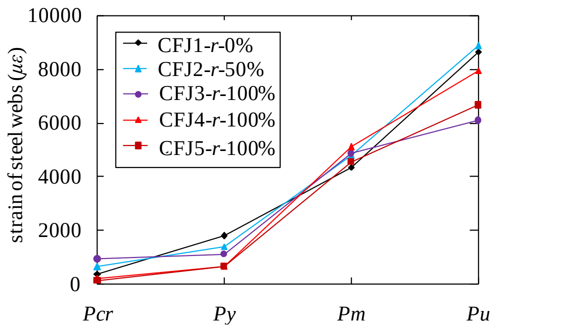

Fig. 8 Strain of the steel webs of joints area at the main state

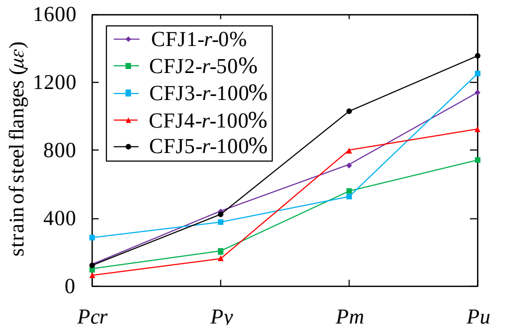

Fig. 9 Strain of the steel flanges of joints area at the main state

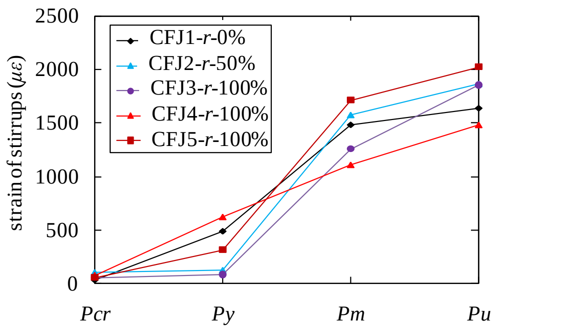

Fig. 10 Strain of the stirrups of the joints area at the main state

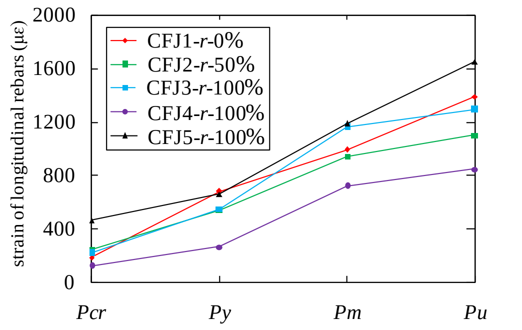

Fig. 11 Strain of the longitudinal rebars of the joints area at the main state

Table 4 Shear force proportion of the main shear elements in the joints

Specimen number	Characteristic loads	V_j^t/kN	V_w^t/V_j^t	V_{sv}^t/V_j^t	V_{rc}^t/V_j^t
CFJ1	P_{cr}	262.9	4.5%	0.5%	95.0%
	P_y	476.6	12.0%	4.4%	83.6%
	P_m	619.0	24.9%	10.2%	64.9%
CFJ2	P_{cr}	252.1	9.1%	0.9%	90.0%
	P_y	442.1	10.2%	3.0%	86.8%
	P_m	589.2	27.7%	12.4%	59.9%
CFJ3	P_{cr}	293.2	10.6%	1.5%	87.9%
	P_y	478.5	10.0%	3.2%	86.8%
	P_m	556.7	28.7%	12.0%	59.3%
CFJ4	P_{cr}	194.0	3.1%	1.1%	95.8%
	P_y	333.7	6.7%	1.0%	92.3%
	P_m	526.4	32.7%	10.1%	57.2%
CFJ5	P_{cr}	263.9	1.4%	1.1%	97.5%
	P_y	395.3	5.5%	6.7%	87.8%
	P_m	613.9	25.0%	7.7%	67.3%

*Note: P_{cr} - Crack load of joint; P_y -Yield load of joint; P_m - Peak load of joint

moment above the central axis of the steel webs section in the column; τ_w is the shear force of the steel webs of the column at the centre; E and G_w are the elastic modulus and the shear elastic modulus of the steel webs of the column, respectively; γ_w and μ are the shear strain and Poisson's ratio of the steel webs of the column, respectively, where γ_w can be obtained from the mechanical formula of the material; a is the same section of the total number of stirrups; E_{sv} and $\bar{\varepsilon}_{sv}$ are the elastic modulus and average strain of the stirrups, respectively; A_{sv1} is the single stirrup sectional area in the same section of the column.

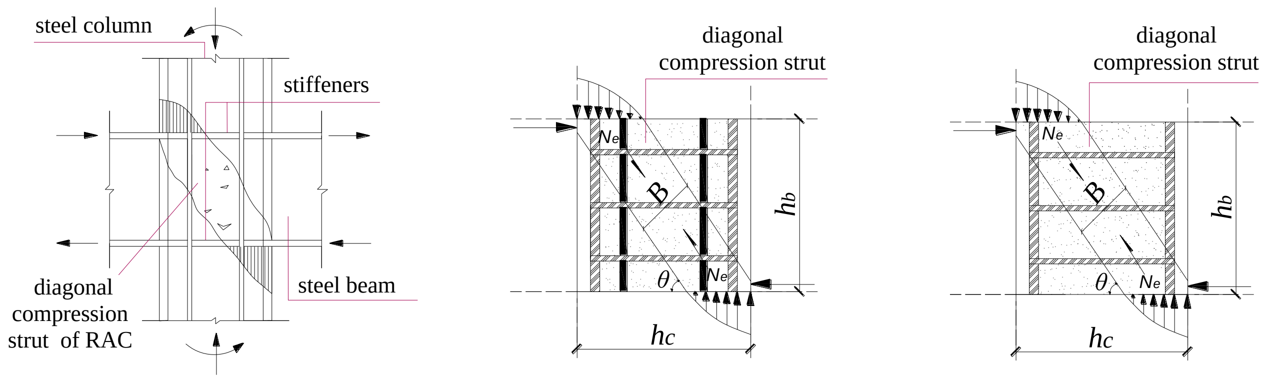

(a) Diagonal compression strut model (b) Diagonal compression strut model in the core area (c) Diagonal compression strut model in the non-core area

Fig. 12 Diagonal compression strut model of the RAC in joints area

4. Shear mechanism of composite frame joints

The research on the shear mechanism of the frame joints can reveal the way of force transmission and distribution of the joints under cyclic loading, and can provide the reasonable theoretical assumptions and calculation model for the shear bearing capacity of the joints. Based on the above mentioned analysis, the shear elements in the joint area were mainly composed of RAC, steel webs and stirrups with a shear-bearing capacity of V_{rc}^{c}, V_{w}^{c} and V_{sv}^{c}, respectively. Therefore, based on existing researches and building codes (Zhao 2001, AISC 1997, AIJ 1994), the nominal shear bearing capacity of the composite frame joints can be expressed as

$$V_j^c = V_{rc}^c + V_w^c + V_{sv}^c \tag{5}$$

4.1 Shear bearing capacity of RAC

Before the cracking of the joints, the pressure generated by the bending moment of the column end and beam end was transmitted to the joint area, so that RAC in the joint area formed compression band along the diagonal direction of the joints, and the tensile stress was produced at the edge of the compression band that is perpendicular to the length direction of the compression band. The joint area produced cracks diagonally and formed the RAC diagonal compression strut gradually given the increase in lateral load. Clearly, the shear bearing capacity of the RAC in the joint area depended on the compressive strength of the RAC diagonal compression strut. Therefore, the shear mechanism of the RAC in the joint area can be replaced by a diagonal compression strut mechanism. Fig. 12 illustrates the force diagrams. The RAC diagonal compression strut in the joint area was divided into two parts, namely, the core area and the non-core area.

According to the principle of diagonal compression strut, the shear bearing capacity equation of the RAC in the joint area can be expressed as

$$V_{rc}^c = N_e \cos\theta \tag{6}$$

where θ is the angle between the diagonal compression strut and horizontal direction; N_{e} is the compressive strength of the diagonal compression strut which can be calculated as follows

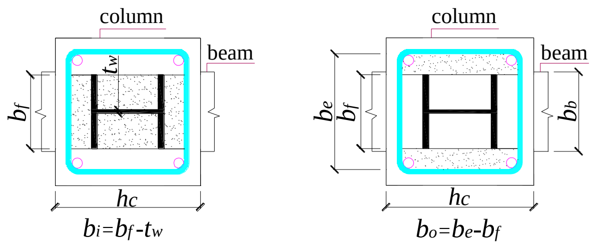

Fig. 13 The width of the diagonal compression strut of the core area and non-core

$$N_e = B\left(b_i f_{rc,i} + b_o f_{rc,o}\right) \tag{7}$$

where b_i and b_o are the width of the diagonal compression strut of the core area and non-core of the joints, respectively. Fig. 13 presents the computing method of the width of the diagonal compression strut of the core area and non-core. In addition, $f_{rc,i}$ and $f_{rc,o}$ are the effective compressive strength of the RAC diagonal compression strut of the core area and the non-core area, respectively.

For the RAC in the core area of joint, the compressive strength of RAC can be effectively improved considering the constraints of the profile steel and stirrups, which can be expressed by the increasing factor k_{c}. Elnashai and Elghazouli (1993) demonstrated that the increasing factor $k_{\mathrm{c}} = 2$ represented a lower bound for the constraint effect of the profile steel to ordinary concrete. Therefore, the paper conservatively considers the lower bound value. The study of Vecchio and Collins (1986) showed that the principal tensile stress perpendicular to the principal compressive stress exerted an adverse effect on the compressive strength of concrete after concrete cracking and proposed the reduction factor β as follows

$$\beta = \frac{1}{0.85 - 0.27\varepsilon_1 / \varepsilon_c'} \tag{8}$$

where ε_1 and ε_c' are the principal tensile strains and the principal compression strains of the concrete, respectively.

Parra-Montesinos and Wight (2001) defined the factor $k_{tc} = -\varepsilon_1/\varepsilon_c'$. Therefore, Eq. (8) can be defined as

$$\beta = \frac{1}{0.85 + 0.27k_{tc}} \tag{9}$$

where the values of k_{tc} primarily depend on the amount of confinement provided to the joint area. For the well-confined joints, the low values of k_{tc} are expected. For the lightly confined joints, the tensile strains will increase rapidly compared with the compression strains, thereby leading to high values of k_{tc}. The average tensile strains are governed by the crack opening rather than the tensile strains of concrete after a significant cracking occurred in the joints. Parra-Montesinos and Wight (2001) adopted $k_{tc} = 3$ and obtained the reduction factor $\beta \approx 0.6$. The value was used as the lower limit of the compressive strength of concrete that is affected by the cracks. Considering the discreteness of RAC material, so the paper used $\beta = 0.6$. In addition, the compression stress produced by the RAC diagonal compression strut was not evenly distributed, as exhibited in Fig. 14, and can be expressed by the nonuniformity factor Ψ. Referring to the provisions of Jia *et al*. (2013) for ordinary steel-reinforced concrete, the value of Ψ can be took 0.75.

Therefore, the effective compressive strength of the RAC diagonal compression strut in the core area of the joint can be expressed as follows

$$f_{rc,i} = \Psi\beta k f_{rc} = 0.75 \times 0.6 \times 2 \times f_{rc} = 0.9 f_{rc} \tag{10}$$

For the RAC in the non-core area of joint, only consider the constraints of stirrups. The study of Parra-Montesinos and Wight (2001) showed that the value of k_c can be taken as 1.1 when the joints were confined only by stirrups. The reduction factor β and nonuniformity factor Ψ were taken according to the above values. Therefore, the effective compressive strength of the RAC diagonal compression strut in the non-core area of the joint can be expressed as follows

$$f_{rc,o} = \Psi\beta k f_{rc} = 0.75 \times 0.6 \times 1.1 \times f_{rc} \approx 0.5 f_{rc} \tag{11}$$

In Eq. (7), B is the width of the RAC diagonal compression strut. Bao (2014) demonstrates that B can be

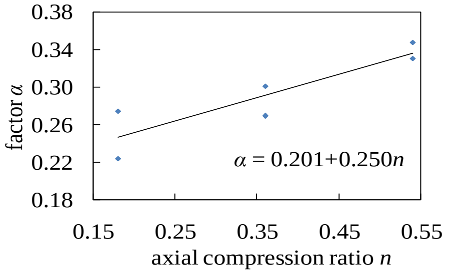

Fig. 14 Relation between shear influence factor and axial compression ratio in the joints

expressed as a ratio of the diagonal of joint area

$$B = \gamma\sqrt{h_j^2 + h_b^2} \tag{12}$$

where h_j is the height of the cross-section of the joint area and typically equal to the cross-sectional height of column h_c; h_b is the cross-sectional height of the beam, which can be expressed as a ratio of the height of the cross section of the column, that is, $h_b = \omega h_c$. Therefore, B can also be expressed as

$$B = \gamma\sqrt{1+\omega^2}\, h_c \tag{13}$$

Therefore, the shear bearing capacity of the RAC in the joint area can be expressed as

$$\begin{aligned} V_{rc} &= N_e\cos\theta = B\left(b_i f_{rc,i} + b_o f_{rc,o}\right)\cos\theta \\ &= \gamma\sqrt{1+\omega^2}\, h_c\cos\theta\left(b_i f_{rc,i} + b_o f_{rc,o}\right) \end{aligned} \tag{14}$$

Substituting $\alpha = \gamma\sqrt{1+\omega^2}\cos\theta$ into the Eq. (14), the shear bearing capacity of the RAC in the joint area is

$$\begin{aligned} V_{rc}^c &= \alpha h_c\left(b_i f_{rc,i} + b_o f_{rc,o}\right) \\ &= \alpha h_c\left[\left(b_f - t_w\right)0.9 f_{rc} + \left(b_e - b_f\right)0.5 f_{rc}\right] \end{aligned} \tag{15}$$

where α is the factor, which can be considered as the shear influence factor. The factor is significantly influenced by the axial compression ratio of the joints and can be obtained using the test values by the Eq. (16). α is as follows

$$\alpha = \frac{V_j^t - V_w^t - V_{sv}^t}{h_c[(b_f - t_w)0.9 f_{rc} + (b_e - b_f)0.5 f_{rc}]} \tag{16}$$

The relationship between factor α and axial compression ratio n was obtained by the linear regression and fitting based on the test data as displayed in Fig. 14. In order to simplify the calculation and analysis, the relationship between factor α and axial compression ratio n can be expressed as follows

$$\alpha = 0.2 + 0.25n \tag{17}$$

In addition, the test results show that the shear bearing capacity of the joint area gradually decreased with the increase in the RCA replacement percentage, thereby indicating that the RCA replacement percentage has a certain adverse impact on the shear bearing capacity of the joint. Therefore, considering the unfavourable effect of the RCA replacement percentage on the shear bearing capacity of the joint is necessary, this effect can be expressed by factor η. The relationship between the factor η and the RCA replacement percentage through the linear regression and fitting based on the test data can be expressed as follows

$$\eta = 1 + 0.074r^2 - 0.125r \tag{18}$$

Substituting Eqs. (17)-(18) into Eq. (15), the shear force provided by RAC in the joints area can be obtained

$$
\begin{aligned}
V_{rc}^{c} &= \eta \alpha h_c \delta_j \left(b_i f_{rc,i} + b_o f_{rc,o}\right) \\
&= \left(1 + 0.074r^2 - 0.125r\right)\left(0.2 + 0.25n\right) h_c \delta_j \\
&\quad \left[\left(b_f - t_w\right) 0.9 f_{rc} + \left(b_e - b_f\right) 0.5 f_{rc}\right]
\end{aligned} \tag{19}
$$

where δ_j is the factor of the joint form, and the inner joints can take 1.0.

4.2 Shear bearing capacity of steel webs

The shear resistance of the steel webs in the core area of the joint gradually increased after the RAC cracking in the joint area. For easy calculation, the steel webs in the joint area can be regarded as a steel 'frame-shear wall' system, as illustrated in Fig. 15.

In Fig. 15, the steel webs of the column in the joint area can be considered a shear wall, and the steel flanges of the column and stiffeners are regarded as a closed frame, thereby forming the steel 'frame-shear wall' system to bear the shear force. The anti-lateral stiffness of the steel flanges of the column is much smaller than that of the steel webs when the steel 'frame-shear wall' system is subjected to shear force. This result indicates that the steel webs in the joint area play a major role in resisting shear force. The steel 'frame-shear wall' system under cyclic loading is in the force state of compressive stress and shear stress, as depicted in Fig. 16 (a).

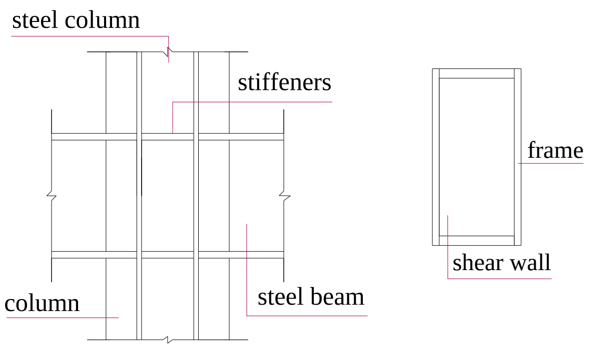

(a) Profile steel in joints area (b) Steel flanges frame in joints area

Fig. 15 Diagram of steel of frame-shear wall in joints

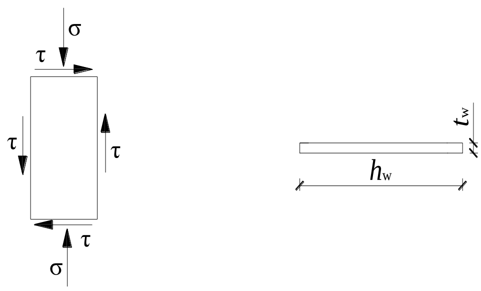

(a) Force diagram of steel webs (b) Thickness and height of steel webs

Fig.16 Force model of steel webs in joints area

The principal stress can be expressed as follows when the profile steel was in the elastic state

$$\sigma_1 = \frac{\sigma}{2} + \sqrt{\left(\frac{\sigma}{2}\right)^2 + \tau^2} \tag{20}$$

$$\sigma_2 = 0 \tag{21}$$

$$\sigma_3 = \frac{\sigma}{2} - \sqrt{\left(\frac{\sigma}{2}\right)^2 + \tau^2} \tag{22}$$

where σ is the axial stress of steel webs; σ_1, σ_2 and σ_3 are the first, second, third principal stresses of steel webs, respectively.

Mises yield criterion can be expressed as follows when the joint reached the ultimate state

$$f_y = \sqrt{\frac{1}{2}\left[\left(\sigma_1 - \sigma_2\right)^2 + \left(\sigma_2 - \sigma_3\right)^2 + \left(\sigma_1 - \sigma_3\right)^2\right]} \tag{23}$$

where f_y is the uniaxial tensile yield strength of the steel webs.

The shear stress at the yield state of the steel webs is expressed as follows by substituting Eqs. (20)-(22) into Eq. (23)

$$\tau_y = \sqrt{\frac{f_y^{\,2} - \sigma^2}{3}} \tag{24}$$

Eq. (24) denotes that the axial stress can reduce the shear bearing capacity of the steel webs. This phenomenon is unfavourable to the shear stress of the steel webs. However, according to the research results of Zhao (2001), the adverse effect of axial stress on the shear strength of the steel webs was relatively small and can be ignored. Therefore, the shear stress of the steel webs can be expressed as follows

$$\tau_y = \frac{f_y}{\sqrt{3}} \tag{25}$$

The shear force provided by the steel webs in the core area of the joint can be obtained as follows

$$V_w^c = \frac{1}{\sqrt{3}} t_w h_w f_y \tag{26}$$

where V_w is the shear bearing capacity of the steel webs in the joint area; t_w and h_w are the thickness and height of the steel webs in the joint area, respectively; f_y is the yield strength of the steel webs.

4.3 Shear bearing capacity of transverse stirrups

The strain of the stirrups in the joint area increased rapidly after the steel webs yielding, thereby indicating that the stirrups play a favourable role in confining the RAC in the joint area and preventing the longitudinal rebars buckling. The stirrups and longitudinal rebars in the joint

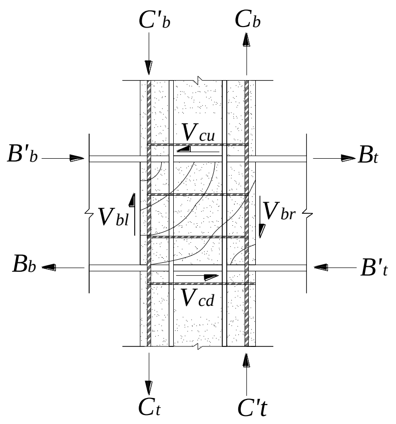

Fig. 17 Mechanism of rebars in the core area of joints

area form a truss system, as illustrated in Fig. 17.

In Fig. 17, $B_b^{'}$, $B_t^{'}$ and B_b, B_t are the stress and tension of the steel flanges of the steel beams, respectively; $C_b^{'}$, $C_t^{'}$ and C_b, C_t are the stress and tension of the longitudinal rebars, respectively; V_{bl}, V_{br} and V_{cu}, V_{cd} are the shear forces of the beams and columns in the joints, respectively.

According to the above strain analysis, the stirrups were one of the three main shear elements in the joints. In addition, the shear effect of the longitudinal rebars can be disregarded for ease of calculation. Therefore, the shear force provided by the truss system of the rebars can be expressed as follows

$$V_{sv}^{c} = A_{sv} f_{yv,e} \tag{27}$$

where $f_{yv,e}$ is the effective yield strength of the stirrups in the joint area; A_{sv} is the cross section of the stirrups in the joint area.

The research results of Park and Milburn (1983) showed that the shear efficiency of the stirrups near the middle area of the joints was more effective than the stirrups near the longitudinal rebars of the beam. Jia *et al*. (2013) suggested that the effective yield strength of the stirrups in the 50% height range of the middle part of the joint was taken as its actual yield strength. All the stirrups in the composite frame joints area in this test were within this range. In addition, the average strain of the stirrups in joint area was 1771 $\mu\varepsilon$, which is approximately 90% of the yield strain of the stirrups, when the peak value of the joints is reached. Therefore, the effective yield strength of the stirrups in the joint area is 90% of the actual yield strength.

Based on the above analysis, the calculated formula of the shear bearing capacity of the composite frame inner joints can be summarized as follows

$$\begin{aligned} V_j^c &= V_{rc}^c + V_w^c + V_{sv}^c \\ &= \eta\alpha h_c \delta_j \left(b_i f_{rc,i} + b_o f_{rc,o}\right) + \frac{1}{\sqrt{3}} t_w h_w f_y + A_{sv} f_{yv,e} \end{aligned} \tag{28}$$

Table 5 summarizes the shear force of each shear element in the joint area and the comparison of the shear bearing capacity of joints between the calculated results and the test results. In Table 5, the average value of the ratio of the calculated results and test results is 0.981, the standard deviation and variation coefficient and are 0.014, 0.014, respectively. The calculated results are in good agreement with the test results. Therefore, the above calculation formulas can be adopted to evaluate the shear strength of the composite frame inner joints of the SRRC column–steel beam.

5. Conclusions

The failure modes, hysteresis curves, strains in joint area and shear mechanisms of the joints were analysed in detail through the cyclic loading test of the composite frame inner joints of the SRRC column–steel beam. Based on this analysis, the formula method of the shear bearing capacity of the joints was proposed in this paper. The main conclusions are as follows:

- The failure process of the joint area can be divided into the elastic stage, working with crack stage and failure stage. The X-shaped diagonal cracks were formed as marked feature in the joint area. The failure modes of the joints can be summarized as a typical shear failure.
- The hysteresis curves of the joints were spindle-shaped and plump, thus indicating that the composite frame inner joints have relatively favourable energy dissipation capacity. The shear bearing capacity of the joints decreased gradually with the increase in the RCA replacement percentage, and the maximum decrement was 10.07%. By contrast, the shear bearing capacity of the joints increased obviously whilst the axial compression ratio increased, and the maximum increment was approximately 16.6%.
- The shear bearing capacity of the joint area was mainly provided by RAC, steel webs and transverse

Table 5 Comparison of calculated values and experimental values of the shear bearing capacity for the joints

Specimen	r /%	n	V_{rc}^c/kN	V_{sv}^c/kN	V_w^c/kN	V^c/kN	V_j^t/kN	V^c/V_j^t
CFJ1	0	0.36	391.5	75.8	149.2	616.4	619.0	0.996
CFJ2	50	0.36	361.9	75.8	149.2	586.9	589.2	0.996
CFJ3	100	0.36	328.5	75.8	149.2	553.4	556.7	0.994
CFJ4	100	0.18	277.5	75.8	149.2	502.4	526.4	0.954
CFJ5	100	0.54	379.4	75.8	149.2	604.4	613.9	0.984

stirrups. More than 95% of the shear force was provided by the RAC in the joint area before cracking. The shear force provided by the steel webs and stirrups increased rapidly after cracking and played a major role in resisting the shear force. The shear strength of the joints after peak loads was reduced slowly owing to the contribution of the steel webs and stirrups in the joint area.

- The calculation model of the shear bearing capacity of joint area was established on the basis of the analysis of the shear mechanism of joints, thereby reasonably reflecting the effect of the RCA replacement percentage and axial compression ratio on the shear strength of the joints. The calculated results of the shear bearing capacity of the joints are in good agreement with the test results. However, further investigations must be conducted to verify the effectiveness of the calculation formulas.

Acknowledgments

The research was financially supported by the National Natural Science Foundation of China P.R. (No.51408485), China Postdoctoral Science Foundation Funded Project (No. 2015M572584), the Plan Projects of the Department of Housing and Urban-rural Development of Shaanxi Province (No.2015-K129), Shaanxi Province Postdoctoral Science Foundation Funded Project and the Project Supported by Natural Science Basic Research Plan in Shaanxi Province of China (No.2016JQ5024), which is gratefully acknowledged.

References

AIJ (1994), AIJ design guidelines for composite RCS joint; AIJ Composite RCS Structures Sub-Committee; Tokyo, Japan.

AISC (1997), Seismic provision for structural steel buildings, American Institute of Steel Construction; Chicago, IL, USA.

Bao, Y.Z. (2014), "Experimental research on seismic performance of steel reinforced recycled concrete frame inner joints", Xi'an University of Architecture and Technology, Xi'an, China.

Breccolotti, M. and Materazzi, A.L. (2010), "Structural reliability of eccentrically-loaded sections in RC columns made of recycled aggregate concrete", *Eng. Struct.*, **32**(11), 3704-3712.

Chen, H.J., Yen, T. and Chen, K.H. (2003), "Use of Building Rubbles as Recycled Aggregates", *Cement Concrete Res.*, **17**(33), 125-132.

Chen, J., Wang, Y.Y. and Roeder, C.W. (2017), "Behavior of normal-strength recycled aggregate concrete filled steel tubes under combined loading", *Eng. Struct.*, **130**(1), 23-40.

Elnashai, A.S. and Elghazouli, A.Y. (1993), "Performance of composite steel/concrete members under earthquake loading. Part I: analytical model", *Earthq. Eng. Struct. Dyn.*, **22**(4), 315-345.

Gonzalez, V.C.L. and Moriconi, G. (2014), "The influence of recycled concrete aggregates on the behavior of beam–column joints under cyclic loading", *Eng. Struct.*, **60**(2), 148-154.

Huda, S.B. and Alam, M.S. (2014), "Mechanical behavior of three generations of 100% repeated recycled coarse aggregate concrete", *Constr. Build. Mater.*, **65**(8), 574-582.

Ignjatović, I.S., Marinković, S.B. and Tošić, N. (2017), "Shear behaviour of recycled aggregate concrete beams with and without shear reinforcement", *Eng. Struct.*, **141**(6), 386-401.

Jia, J.Q., Zhu, W.Q. and Wang, J.Z. (2013), "Shear strength of interior steel reinforced high strength concrete beam-column joints", *China Civ. Eng. J.*, **46**(10), 1-8.

Marthong, C., Sangma, A.S. and Choudhury, S.A. (2017), "Structural behavior of recycled aggregate concrete beam-column connection in presence of micro concrete at joint region", *Structures*, **11**(8), 243-251.

Park, R. and Milburn, J.R. (1983), "Comparison of recent New Zealand and United States seismic design provisions for reinforced concrete beam-column joints and test results from four units designed according to the New Zealand Code", *Bulletin of the New Zealand National Society for Earthquake Engineering*, **16**(1), 3-24.

Parra-Montesinos, G. and Wight, J.K. (2001), "Modeling shears behavior of hybrid RCS beam-column connections", *J. Struct. Eng.*, **127**(1), 3-11.

Poon, C.S., Kou, S.C. and Lam, L. (2002), "Use of recycled aggregates in molded concrete bricks and blocks", *Constr. Build. Mater.*, **16**(5), 281-289.

Rosado, L.P., Vitale, P., Penteado, C.S.G. and Arena, U. (2017), "Life cycle assessment of natural and mixed recycled aggregate production in Brazil", *J. Cleaner Prod.*, **151**(5), 634- 642.

Senaratne, S., Lambrousis, G. and Mirza, O. (2017), "Recycle concrete in structural Applications for sustainable construction Practices in Australia", *Proc. Eng.*, **180**(4), 751-758.

Šeps, K., Fládr, J. and Broukalová, I. (2016), "Resistance of recycled aggregate concrete to freeze-thaw and deicing salts", *Pro. Eng.*, **151**(7), 329-336.

Silva, R.V., de Brito, J. and Dhir, R.K. (2016), "Establishing a relationship between modulus of elasticity and compressive strength of recycled aggregate concrete", *J. Cleaner Prod.*, **112**(1), 2171-2186.

Thomas, C., Setién, J. and Polanco, J. (2013), "Durability of recycled aggregate concrete", *Constr. Build. Mater.*, **40**(3), 1054 -1065.

Ma, H., Xue, J.Y. and Zhang, X.C. (2013), "Seismic performance of steel-reinforced recycled concrete columns under low cyclic loads", *Constr. Build. Mater.*, **48**(11), 229-237.

Ma, H., Xue, J.Y. and Liu, Y.H. (2015), "Cyclic loading tests and shear strength of steel reinforced recycled concrete short columns", *Eng. Struct.*, **92**(6), 55-68.

Ma, H., Xue, J.Y. and Liu, Y.H. (2016), "Numerical analysis and horizontal bearing capacity of steel reinforced recycled concrete columns", *Steel Compos. Struct., Int. J.*, **22**(4), 797-820.

Vecchio, F.J. and Collins, M.P. (1986), "The modified compression -field theory for reinforced concrete elements subjected to shear", *ACI Journal*, **83**(2), 219-231.

Wu, B., Zhao, X.Y and Yang, Y. (2013), "Seismic test and numerical simulation of with recycled concrete columns with thin walled circular steel tubes-reinforced concrete beams joints", *China Civ. Eng. J.*, **46**(3), 59-69.

Xiao, J.Z. (2008), *Recycled Concrete*, Architecture & Building Press, Beijing, China.

Xu, J.J., Chen, Z.P. and Xiao, Y. (2017), "Recycled Aggregate Concrete in FRP-confined columns: A review of experimental Results", *Compos. Struct.*, **174**(8), 277-291.

Xue, J.Y., Luo, Z.Y. and Cheng, F. (2010), "Study on mechanical properties and durability of recycled concrete", *Ind. Constr.*, **2**(10), 91-96.

Xue, J.Y., Bao, Y.Z. and Ren, R. (2014), "Experimental study on seismic performance of steel reinforced recycled concrete inner-frame joints under low-cyclic reversed loading", *China Civil Eng. J.*, **47**(10), 1-8.

Yang, Y.F. (2015), "Modeling of recycled aggregate concrete-filled steel tube (RACFST) beam-columns subjected to cyclic loading", *Steel Compos. Struct., Int. J.*, **18**(1), 213-233.

Yoda, K. and Shintani, A. (2014), "Building application of recycled aggregate concrete for upper-ground structural Elements", *Constr. Build. Mater.*, **67**(9), 379-385.
Zhao, Y.T. (2001), *Steel and Concrete Composite Structures*, Science Press, Beijing, China.

CC